CONTROL OF MAGLEV VEHICLES WITH AERODYNAMIC AND GUIDEWAY DISTURBANCES†

Karl Flueckiger, Steve Mark, and Ruth Caswell
The Charles Stark Draper Laboratory, Inc.
Cambridge, MA

Duncan McCallum
Harvard University
Cambridge, MA

SUMMARY

A modeling, analysis, and control design methodology is presented for maglev vehicle ride quality performance improvement as measured by the Pepler Index. Ride quality enhancement is considered through active control of secondary suspension elements and active aerodynamic surfaces mounted on the train.

To analyze and quantify the benefits of active control, the authors have developed a five degree-of-freedom lumped parameter model suitable for describing a large class of maglev vehicles, including both channel and box-beam guideway configurations. Elements of this modeling capability have been recently employed in studies sponsored by the U.S. Department of Transportation (DOT).

A perturbation analysis about an operating point, defined by vehicle and average crosswind velocities, yields a suitable linearized state space model for multivariable control system analysis and synthesis. Neglecting passenger compartment noise, the ride quality as quantified by the Pepler Index is readily computed from the system states. A statistical analysis is performed by modeling the crosswind disturbances and guideway variations as filtered white noise, whereby the Pepler Index is established in closed form through the solution to a matrix Lyapunov equation. Data is presented which indicates the anticipated ride quality achieved through various closed-loop control arrangements.

1. INTRODUCTION

A maglev vehicle's suspension system is required to maintain the primary suspension air gap while minimizing passenger compartment vibrations in the presence of guideway irregularities and aerodynamic disturbances. It must meet these requirements while: (1) minimizing the size of the required air gap so that more efficient lift magnets can be employed; (2) minimizing the

†This work was supported in part by Draper Independent Research and Development (IR&D) Project #463.

stroke length of the secondary suspension so that vehicle frontal area and drag are as small as possible; (3) minimizing the size, weight, and required power of active suspension elements. Unfortunately, these design goals conflict with the desire to increase the allowable guideway roughness (to reduce guideway cost) and maximize crosswind disturbance rejection. Active control offers great potential to improve suspension performance. Constructing a maglev transportation system, or even a short test section, is a very expensive venture. Therefore, it is cost effective to develop analytic tools that can predict trade-offs between the various conflicting system requirements and performance metrics. This allows design alternatives to be examined before building either an actual system or scale model. Unfortunately, the scaling properties associated with magnetic systems preclude construction of accurate maglev vehicle scale models.

In this paper we describe a modeling, analysis, and control design methodology specifically for ride quality improvement as measured by the Pepler Index. We consider a generic EDS type maglev vehicle having a null flux primary suspension and bogies. This is a variation of the vehicle proposed by the Bechtel consortium's System Concept Definition (SCD) study [1]. The model incorporates front and rear bogies, each having roll but no pitch or yaw dynamics. The guideway disturbance is modeled in three directions (vertical, lateral, and roll) as linear systems driven by white noise. A crosswind disturbance, which acts against the side of the vehicle, is also modeled in this fashion. We consider control authority produced by an active secondary suspension consisting of actively controlled elements (hydraulic or electro-mechanical actuators) that exert forces between the vehicle and its suspension bogies. We also analyze the potential benefits of actively controlled aerodynamic surfaces implemented in conjunction with the conventional secondary suspension. The aerodynamic control surfaces considered here are winglets that exert forces directly on the vehicle body, which, due to high vehicle operating speeds, can produce reasonably large forces when modestly sized. Aerodynamic control surfaces have the advantage of exerting forces directly on the vehicle without exerting reaction forces on the bogies.

Wormley and Young developed a heave and pitch model of a vehicle subjected to simultaneous guideway and external (such as wind) disturbances [2]. A methodology for optimizing the passive suspension performance in the presence of these simultaneous disturbances was derived and the results evaluated. Guenther and Leonides developed a multiple degree-of-freedom model for a maglev vehicle that includes front and rear bogies, with a time-delayed guideway disturbance to the rear bogie [3]. A control system was developed based on the solution to the stochastic optimal control problem. Gottzein, Lange, and Franzes developed a secondary suspension model with an active control system for a Transrapid type EMS vehicle [4]. A Linear Quadratic Gaussian (LQG) controller was developed for the vertical direction.

The research presented here is a natural extension of the works cited above to provide an integrated five degree-of-freedom model that includes guideway irregularities and aerodynamic effects. The remainder of this paper is organized as follows: §2 contains an overview of the model employed in our analysis; §3 hosts a discussion of the control system analysis and design methodology employed by the authors to obtain results given in §4; §5 concludes with summary remarks about and consequences of our findings.

2. ANALYSIS MODEL OVERVIEW

Key elements of the analytic model developed for ride quality analysis and control system synthesis are presented within this section. Assumptions imbued in the modeling process are

stated explicitly. However, for the sake of brevity, a rigorous treatment of vehicle dynamics is not developed here. The interested reader is referred to [1],[5], and [6] for more lengthy discussions.

A depiction of the maglev system under discussion is given in Fig. 1, which shows the vehicle body suspended on two bogies. The bogies contain superconducting magnets required for the primary suspension which suspends the bogies relative to the guideway. The secondary suspension is composed of passive spring and damper elements as well as active components that exert forces between the bogies and the vehicle body. We assume that the primary and secondary suspension elements exert forces in the vertical and lateral directions, as well as roll torques. Additional control authority is provided by six active aerosurfaces mounted on the train.

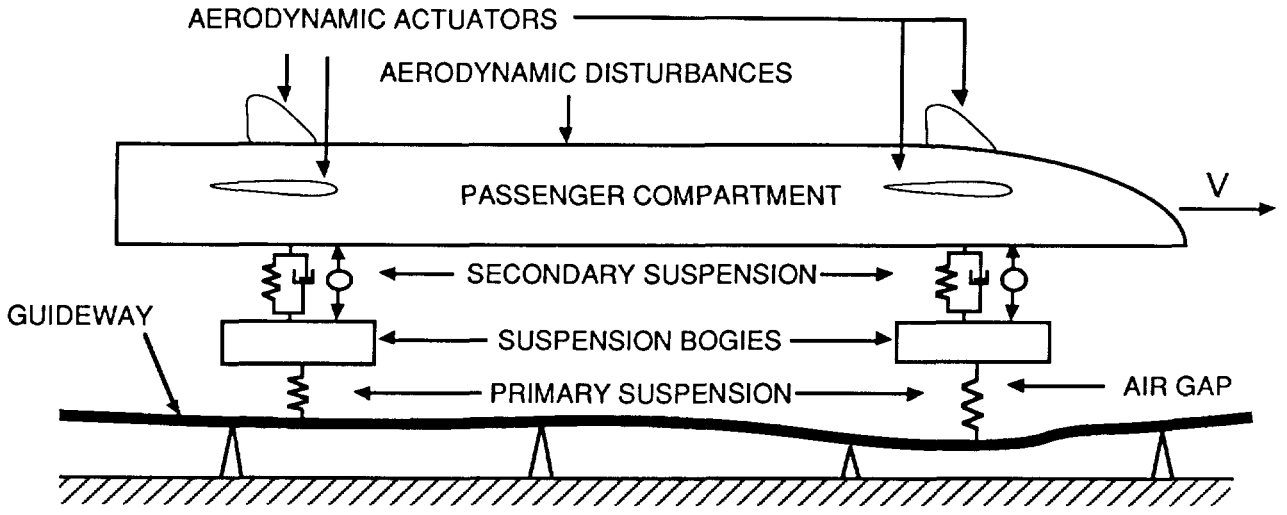

Figure 1. Maglev Vehicle Concept.

Disturbances to the system are guideway irregularities and aerodynamic forces due to crosswinds. The guideway is assumed to be perfectly rigid, but with an irregular surface that can be described by three sets of independent statistics: one each for vertical, lateral, and roll disturbances. For analysis purposes, we assume a worst case scenario where crosswind disturbances act in the lateral direction.

We assume that the vehicle forward velocity, V, is constant and that there is no coupling between the magnetic propulsion and levitation systems. The vehicle body and bogies are permitted to move in the vertical and lateral directions, and also to roll. The vehicle body has the additional freedom to yaw and pitch. Variations about the vehicle's forward velocity are not included in the model. The allowable directions of motion are sketched in Figures 2 and 3, where the variable y represents the lateral direction, z vertical, ϕ roll, θ pitch, and ψ yaw. The lack of bogie yaw and pitch dynamics is not seen to be a major analytic deficiency. Due to the large moment arm about the vehicle body's center of gravity (CG), the torque on the vehicle body caused by bogie yawing is expected to be small compared to that due to lateral displacement of the bogie. A similar argument applies to the omission of bogie pitch dynamics. In conjunction with this restriction, there is no finite magnet length filtering of the guideway disturbances, as might be the case for an actual vehicle.

The following additional assumptions are made: the vehicle body's and bogies' CGs are in the geometric center of the respective bodies, both laterally and longitudinally; the vehicle body and bogies are completely rigid; the passengers and their baggage are fixed to the vehicle body; both bogies have identical dimensions, mass properties, and primary suspension stiffnesses; and small angle approximations are valid throughout the linear suspension model when relating linear to angular displacements.

The maglev vehicle's physical parameter values in our analyses are similar to a box-beam guideway design developed by the Bechtel consortium for the U.S. Department of Transportation [1]. Representative gross physical properties are summarized in Table 1. The remainder of this section consists of a brief synopsis of the suspension force models followed by a discussion of the active aerodynamic surfaces considered. The section is concluded with descriptions of the guideway and crosswind disturbance models utilized.

A. Suspension Forces

To obtain a suitable linear system description, we model the maglev vehicle in a lumped mass fashion. All suspension elements are modeled as massless generalized springs. For example, the suspension force, **F**, due to the displacement between the front bogie and the guideway is determined by the relationship below:

$$\mathbf{F} = \mathbf{K}\mathbf{r} + \mathbf{D}\dot{\mathbf{r}} \tag{1}$$

where **K** is the spring stiffness matrix, **D** is the damping, and **r** is the equilibrium displacement vector. The spring constants for the primary suspension system are dependent upon forward velocity; representative values as a function of train speed are given in Table 2. Damping for this type of magnetic suspension is believed to be very low [7] and therefore is assumed zero for modeling purposes. Passive secondary suspension spring constants and damping ratios are selected to improve ride quality while simultaneously preventing touchdown and limiting the active secondary suspension stroke. The optimization procedure is discussed in §3.

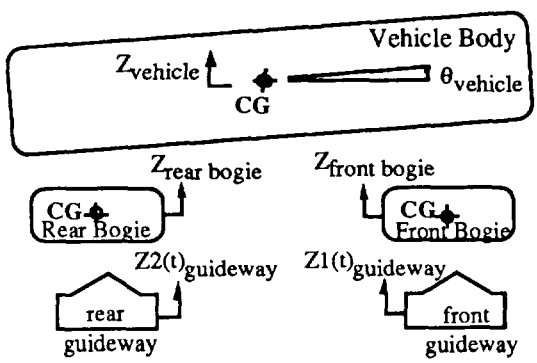

Figure 2. Degrees of Freedom: Side View

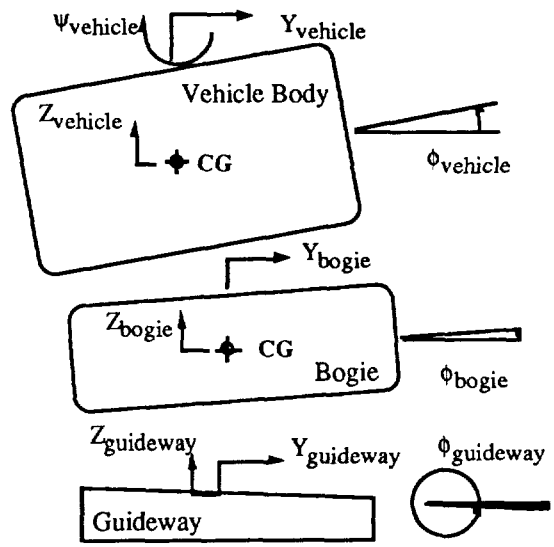

Figure 3. Degrees of Freedom: Front View.

Table 1
Representative Physical Dimensions

Parameter	Value
Vehicle Height	4.9m
Vehicle Length	36.1m
Vehicle Width	3.7m
Total Mass	64400kg
Passenger Compartment Mass	40830kg
Distance Between Bogies	18.7m
Bogie Height	0.75m
Bogie Width	1.5m
Top Winglet CP to Train CG (vertical)	2.3m
Side Winglet CP to Train CG (horizontal)	2.4m

Table 2
Primary Suspension Stiffness

Vehicle Speed	Lateral Stiffness	Vertical Stiffness
50.0 m/s	-1.09e7 N/m	-3.23e7 N/m
134.0 m/s	-1.35e7 N/m	-3.97e7 N/m
150.0 m/s	-1.36e7 N/m	-4.01e7 N/m

It is assumed that all suspension forces act in equal and opposite directions across the gap between the elements under consideration. For simplicity, we model these forces as being applied to fixed points relative to the guideway's, bogies', and passenger compartment's centers of gravity.

B. Aerodynamic Actuation

Six active aerodynamic surfaces, as shown in Figure 1, are available to the control system for improving ride quality. We assume that these actuators operate in "free-stream" and are modeled as winglets with one degree-of-freedom. Four winglets are mounted on the sides of the train and produce vertical forces at the surfaces' centers of pressure (CP): two in front on opposite sides, and two in back on opposite sides. Two winglets are mounted on the top of the train (in "rudder-like" arrangements) to provide lateral forces.

The lift force for a flap in free-stream is given by:

$$F_L = \frac{1}{2}\rho |V_{air}|^2 A C_L(\alpha) \qquad (2)$$

where ρ is air density, A is area, V_{air} is the velocity of the air mass relative to the winglet, and α represents angle of attack. We consider only the lift component of the flap forces. The induced drag of the flaps is calculated to determine the drawbacks of aerodynamic control in [5], but its effect on ride quality is not considered here. Since induced drag acts parallel to the velocity vector, drag forces lie in a direction not included in our model. The lift coefficient is obtained from conventional aerodynamic theory [8] and is nearly linear for small angles of attack. A linear equation for $C_L(\alpha)$ results: $C_L(\alpha) = C_L\alpha$, where $C_L = 0.0264/°$. We assume that V_{air} in (2) is equal to the train's velocity and ignore the effects of crosswind and vehicle rotation. Also, we use a small angle approximation for α to model the lift force as perpendicular to the undeflected winglet surface.

In theory, a very large aerodynamic force can be obtained for relatively low aero-actuator torque. Since the flaps rotate about their centers of pressure, the aerodynamic torques across

flap rotation joints are small when compared to the forces generated by the flaps. However, the actual force required in a hydraulic system that drives a winglet can still be large, due to physical constraints and practical considerations. The dynamics of the closed-loop system may dictate a high actuator bandwidth resulting in large actuator power requirements.

C. System Disturbances

Guideway irregularities are captured by the stochastic model:

$$\Phi_{guideway}(\omega) = \frac{A_r V}{\omega^2} \tag{3}$$

where $\Phi_{guideway}$ is the guideway Power Spectral Density (PSD), A_r is the Roughness Parameter, and V is the train's forward velocity. A roughness parameter corresponding to welded steel rail (gage 4-6) is used to define the guideway PSD, which is subsequently used to form a linear system driven by white noise to describe the guideway position variations. While a typical guideway will not be made of steel and its irregularities as seen by the train will be dominated instead by the misalignment of guideway coils, its roughness parameters are expected to fall in the range of those of welded steel rail. Roughness parameters are given in Table 3.

We assume further that the guideway disturbances act upon the front and rear of the train at the bogie locations. Since the guideway is assumed rigid, the disturbance affecting the rear bogie is identical to that acting on the front bogie, but delayed in time. Therefore, we model the rear guideway dynamics by the time delayed front guideway position variation. Clearly, the time delay is inversely proportional to vehicle forward velocity: $T_{delay} = L/V$, where L is the distance between bogies. Since a time delay cannot be described by an exact finite dimensional continuous time state space representation, a Pade approximation is incorporated into the control system analysis and synthesis model:

$$e^{-sT} \approx \frac{2 + T_{delay}s + \frac{1}{2!}(-T_{delay}s)^2 + \frac{1}{3!}(-T_{delay}s)^3 + \ldots}{2 + T_{delay}s + \frac{1}{2!}(T_{delay}s)^2 + \frac{1}{3!}(T_{delay}s)^3 + \ldots} \tag{4}$$

The crosswind description consists of the sum of two terms: a constant, steady-state mean value and a time variant random process. The mean crosswind velocity is equal to half of the peak crosswind velocity, assuming a maximum three sigma variation from the mean. In our analysis we assume 26.8m/s (60mph) crosswind peak. The PSD of the time varying crosswind component is given by:

$$\Phi_{wind}(\omega) = \frac{2\sigma_w^2 \nu}{\omega^2 + \nu^2} \tag{5}$$

where the break frequency, ν, is 1.0 rad/sec, and the RMS wind velocity, σ_w, is 4.8 m/s (10mph). Φ_{wind} is implemented by a linear system driven by white noise. We assume that the crosswind is perpendicular to the guideway. This maximizes vehicle sideslip, effectively softening the lateral suspension stiffness and thereby degrading system performance.

Table 3
Guideway Roughness Parameters

Parameter	Value
A_r (vertical)	1.2e-6 rad^2-m/s
A_r (lateral)	1.2e-6 rad^2-m/s
A_r (roll)	5.7e-7 rad^4/m-s

3. ANALYSIS

Analysis of the system model begins with choosing the passive secondary suspension's stiffness and damping parameters. The function of the secondary suspension system is to improve ride quality while simultaneously preventing vehicle contact (touchdown) on the guideway. The active secondary suspension stroke must also be kept within practical limits. Typically, the passive suspension parameters cannot be selected to optimize all of these criteria simultaneously, and hence, the parameters are determined through trade-off analyses. Once the suspension elements have been defined, a force balance condition is exploited to determine nominal operating equilibrium values for the vehicle's center of pressure and sideslip angle (given forward and average crosswind velocities). Finally, the linear perturbation model is assembled and a candidate control law synthesized. The resulting closed-loop system is analyzed in a statistical framework. The remainder of this section presents further details of these procedures.

A. Secondary Suspension Parameter Optimization

The primary suspension design involves an inherent conflict between ride quality and guideway tracking. A stiff primary suspension provides improved guideway tracking at the expense of significant guideway and wind disturbance transmission to the passenger compartment. Additionally, a stiff magnetic suspension generally exhibits efficient power consumption. Power considerations, rather than ride quality factors, generally dictate primary suspension design. With the primary suspension parameters assumed given, the secondary suspension parameters are chosen to address the trade-off between the system performance measures of interest, with the overall goal of achieving the best ride quality.

System performance can be evaluated through the root mean squared (RMS) values of relevant quantities in our model. RMS velocity and acceleration levels can be used to compute the Pepler index. The primary air gap and secondary suspension stroke requirements can also be estimated from the RMS variations of these variables, which provides a method of specifying the primary and secondary suspension stroke limits through stochastic control techniques. The motivation behind this treatment stems from the guideway and wind disturbances being characterized by linear systems driven by white noise, whereby it is natural to determine the system outputs for analysis in a similar form.

Details of the trade-off studies used for characterizing the passive secondary suspension system are beyond the scope of this paper, but can be found in [1],[5], and [6]. The design parameter values are listed in Table 4.

Table 4
Passive Secondary Suspension Parameters

Vertical Natural Frequency	0.8 Hz
Vertical Damping Ratio	0.10
Lateral Natural Frequency	1.5 Hz
Lateral Damping Ratio	0.5
Roll Stiffness	0.0 N-m/rad
Roll Damping	2.0e6 N-m-s/rad

B. Operating Point Force Balance

To obtain a linear state space perturbation analysis model, we need to determine the vehicle steady-state sideslip angle, β, and the location of the center of pressure (CP) relative to the CG. This is performed through a force balance analysis, where forces and moments arising from the constant component of crosswind velocity are canceled by the primary and passive suspension systems (Equation (1)). Crosswind forces on the train are modeled as a side force acting at the CP perpendicular to forward velocity. The aerodynamic side force is given by:

$$\left[F_y\right]_{aero} = \frac{1}{2}\rho|V_{air}|^2 A_t C_y(\beta) \tag{6}$$

where A_t is the train's cross-sectional area and $C_y(\beta)$ is the coefficient of side force. The air-relative train velocity, V_{air}, is the vector sum of the train's earth-relative and crosswind velocities. The aerodynamic coefficient, $C_y(\beta)$, is non-linearly dependent on the sideslip angle and is described by a third order polynomial fit to data generated in [5].

Thus, given forward vehicle velocity and steady-state crosswind speed, the aerodynamic forces on the vehicle are computed as a function of β and CP location via (6). A set of nonlinear equations is solved numerically to determine β and CP by balancing $[F_y]_{aero}$ against the nonaerodynamic forces contained in the model, where all time-varying zero mean disturbances and actuator displacements are nulled. For the data presented in §4, the vehicle and mean wind velocities are 150m/s (336mph) and 13.4m/s (30mph) respectively. The resulting steady-state sideslip, β, is 0.092rad (5.27°), which corresponds to a 0.0026rad (0.149°) vehicle yaw angle, ψ.

C. Covariance Analysis

To construct our linear perturbation model, we further assume that the passenger compartment and bogie angular rotation rates are small, and we neglect nonlinear coupling terms due to Coriolis accelerations and gyroscopic effects. The resulting linear equations of motion are placed in state space form, $\dot{\mathbf{x}} = \mathbf{Ax} + \mathbf{Bu} + \mathbf{Fw}$, where: the system state, $\mathbf{x}$, contains train and bogie positions and velocities, and guideway positions (constrained to appropriate degrees of freedom); the system actuator input vector, $\mathbf{u}$, contains active secondary suspension force and aerosurface deflection commands; and the disturbance input vector, $\mathbf{w}$, is (Gaussian) unit intensity white noise.

A measure of ride quality commonly used for maglev vehicles is the Pepler ride quality criteria [9], P.I., which is given by:

$$P.I. = 1.0 + 0.5\sigma_{\dot{\phi}} + 17\sigma_{\ddot{z}} + 17\sigma_{\ddot{y}} + 0.1(dB(N) - 65) \tag{7}$$

where $\sigma_{\dot{\phi}}$ is the passenger RMS roll rate, $\sigma_{\ddot{z}}$ is the passenger RMS vertical acceleration, $\sigma_{\ddot{y}}$ is the passenger RMS lateral acceleration, and dB(N) is the passenger compartment noise level (decibels). Values of the Peplar Index varying from 1 (very comfortable) to 7 (very uncomfortable) provide an indication of perceived ride quality.

In our analysis, we ignore the compartment noise level. Hence, P.I. is a scalar sum of system statistics, which can be denoted $\mathbf{z} = \mathbf{Cx} + \mathbf{Du}$ (ignoring the constant term, 1.0). By defining our analysis variables in this manner, we proceed to design a controller using Linear Quadratic Regulator (LQR) theory, which synthesizes a state feedback control law of form: $\mathbf{u} = -\mathbf{Gx}$. The gain matrix, $\mathbf{G}$, is selected to minimize a quadratic cost functional that includes weighted terms containing performance variables of interest and control energy required. The cost functional, J, provides an optimal trade-off between actuator effort and closed-loop system performance:

$$J = \lim_{T\to\infty} E\left\{\int_0^T \left(\mathbf{z}(t)^T \mathbf{Q}\, \mathbf{z}(t) + \mathbf{u}(t)^T \mathbf{R}\, \mathbf{u}(t)\right) dt\right\} \tag{8}$$

The matrices $\mathbf{Q}$ and $\mathbf{R}$ are used to vary the relative importance of the system outputs and control effort respectively (E denotes the expectation operator). The gain matrix $\mathbf{G}$ minimizing this cost functional is given by:

$$\mathbf{G} = \mathbf{R}^{-1}\left[\mathbf{D}^T\mathbf{QC} + \mathbf{B}^T\mathbf{K}\right] \tag{9}$$

where $\mathbf{K}$ is the solution to an algebraic Riccati equation [10]:

$$\mathbf{KA} + \mathbf{A}^T\mathbf{K} + \mathbf{C}^T\mathbf{QC} - [\mathbf{KB} + \mathbf{C}^T\mathbf{QD}]\mathbf{R}^{-1}[\mathbf{B}^T\mathbf{K} + \mathbf{D}^T\mathbf{QC}] = \mathbf{0} \tag{10}$$

We calculate the closed-loop system steady-state state covariances analytically. If $\mathbf{A_{cl}}$ is the closed-loop system matrix ($\mathbf{A_{cl}} \equiv \mathbf{A} - \mathbf{BG}$), then the state covariance matrix steady-state solution, Σ_{xx}, is the solution to the Lyapunov equation [11]:

$$\mathbf{A_{cl}}\Sigma_{xx} + \Sigma_{xx}\,\mathbf{A_{cl}}^T + \mathbf{FF}^T = \mathbf{0} \tag{11}$$

A system output for analysis, denoted $\mathbf{y}$, is defined as a linear combination of system states: $\mathbf{y} = \mathbf{C_{out}x}$. The output covariance matrix, Σ_{yy}, is given by:

$$\Sigma_{yy} = \mathbf{C_{out}}\,\Sigma_{xx}\,\mathbf{C_{out}}^T \tag{12}$$

The RMS of the output vector, $\mathbf{y}$, is directly computed through the terms along the diagonal of Σ_{yy}. This analysis methodology permits us to compute analytically the statistics of important system properties, such as the Pepler Index, bogie displacements, and actuator commands, without having to resort to Monte Carlo schemes.

4. RESULTS

Results obtained using the analysis model described in §2 are presented here. Control algorithms are developed and the resulting closed-loop systems analyzed as per §3. We select the weighting matrices, **Q** and **R** in (8), to provide good ride quality while maintaining, if possible, the strict suspension gap requirements defined in [1]. Tables 5 through 8 present data indicating basic system performance for four candidate control strategies: (1) no active control (open-loop); (2) active secondary suspension control only; (3) active aerosurfaces only, and (4) active secondary suspension and aerosurfaces (hybrid control). The tables present results associated with guideway disturbances alone, crosswind disturbances alone, and the combination of both sets of disturbances. RMS accelerations are evaluated for passengers seated over the front bogie, at the center of the passenger compartment, and over the rear bogie. These RMS values, along with the RMS roll rate, permit ride quality to be evaluated in terms of the Pepler Index at these three locations.

We assume a forward vehicle velocity of 150m/s (336mph) and a peak crosswind (three-sigma) velocity of 26.8m/s (60mph). The nominal air gaps are 5 cm in the lateral direction and 10 cm in the vertical direction. We desire a five-sigma air gap variation requirement in response to disturbances. This requirement is most difficult to meet at the front of the vehicle, where the steady-sate air gap deviation is 0.85 cm in the lateral and 0.72 cm in vertical direction. For the secondary suspension strokes, the maximum allowable values are 19 cm in the lateral and 10 cm in the vertical direction, and in this case the requirement is relaxed to three-sigma variations. Again, the front of the vehicle has the largest steady-state deviation, 3.19 cm in the lateral direction and 2.43 cm in the vertical direction. Both the air gap variations and secondary suspension strokes are determined at the outside edge of the front and rear bogies.

A. Passive Secondary Suspension

Passive secondary suspension optimization was described in §2. The performance given by the passive system is given in Tables 5 through 8, and is taken as the baseline against which the actively controlled systems are compared. The ride quality, as measured by the Pepler index, is uncomfortable at the front and is tending toward somewhat uncomfortable at the center and rear of the vehicle. The acceleration, air gap, and secondary suspension stroke variations in the lateral direction are all largest at the front of the vehicle due to the location of the center of aerodynamic pressure ahead of the center of gravity. The requirement on the lateral air gap variations is not achievable for any secondary suspension design, and therefore indicates that a basic change in the primary suspension system is necessary. However, for the purposes of this paper, the lateral air gap variations will be minimized as much as possible. Also, although not unreasonable, the 26.8m/s (60mph) peak crosswind velocity assumed for this study is rather high; crosswinds of this level may not be present in all scenarios. However, since the crosswind force is approximately proportional to the product of vehicle velocity and crosswind velocity, a speed restriction during high wind conditions will ameliorate the detrimental effects of crosswinds.

B. Active Secondary Suspension

In this paper, active secondary suspension refers to a configuration where active hydraulic actuators are employed between the vehicle body and the bogies. The active and passive suspension elements are assumed collocated. Note that the RMS acceleration levels for this

system have been reduced when compared to the passive system in both the vertical and lateral directions. Since the passive system has vertical air gap variations which are below the system requirement, the optimal control design methodology was used to achieve smaller vertical accelerations at the expense of larger air gap variations, as discussed in §3. However, in the lateral direction, the passive design exhibited air gap variations which were larger than allowable and so this trade-off could not be utilized. In addition, the authors decided that the control design should not attempt to reduce the lateral air gap variations (relative to those achievable by passive suspension); we do not endorse an EDS vehicle design that depends on the active control system to maintain adequate air gap clearance. A failure of the control system could result in vehicle contact with the guideway.

An important accomplishment of the active secondary suspension is the reduction of the vehicle roll rate by approximately a factor of 10. This is especially significant since roll has been judged to be an especially uncomfortable motion by passengers: half of the roll rate RMS adds directly to the Pepler index. The Pepler index has been reduced by 2.0-2.5 at all three locations along the vehicle. This results in a ride quality which is considered better than average and towards comfortable at the center and rear.

A fundamental disadvantage of the active hydraulic actuators is that any force exerted against the vehicle body to cancel a disturbance will have an equal and opposite reaction force acting against the bogies. Thus there is a direct trade-off between air gap variations, secondary suspension strokes, and vehicle accelerations.

C. Active Aerodynamic Surfaces

The use of active aerodynamic control surfaces results in vertical accelerations which are smaller at all three locations along the vehicle and lateral accelerations which are lower at the center and rear but slightly higher at the front of the vehicle . The ride quality (as measured by the Pepler index) is the same at the front but slightly lower at the center and rear of the vehicle when compared to the active secondary suspension design. It is important to note that this ride quality improvement is obtained without any appreciable increase in the air gap variations, in contrast to the active hydraulic actuator suspension. Compared to the passive system, the secondary suspension strokes are larger, especially in the vertical direction, but remain within acceptable values. The roll rate is slightly less than that of the system with hydraulic actuators.

The primary advantage of the active aerodynamic surfaces is that they exert forces against the vehicle body with respect to an earth fixed (inertial) frame. Therefore, the effects of guideway disturbances on the vehicle body can be minimized without directly affecting the air gap variations. This is equivalent to holding the vehicle body stationary while the bogies bounce beneath it. Of course, this results in larger secondary suspension stroke variations, as illustrated by the data presented. The crosswind forces cannot be canceled directly even though, like the aerodynamic control surfaces, they act directly on the vehicle body. Two primary reasons for this arise because the crosswind disturbance is neither: (1) known beforehand, as the rear guideway disturbances are, nor (2) directly measurable. Another reason stems from non-collocation of crosswind forces and aerodynamic actuators.

The maximum RMS angle of attack of the aerodynamic surfaces was assumed to be 9°, based on the predicted deflection at which the aerodynamic surface stalls. This value was used for all of the aerodynamic surfaces. More control authority for the lateral fin at the front of the vehicle would have provided a greater potential for ride quality improvement. However, the size of the aerodynamic actuators at all locations was limited to practical values.

D. Active Hybrid Suspension

The hybrid active suspension, which incorporates hydraulic actuators between the vehicle body and bogies as well as aerodynamic actuators mounted to the vehicle body, achieves slightly lower lateral accelerations at the front and center of the vehicle when compared to the other active suspension configurations. The acceleration reduction in the lateral direction at the rear, and in the vertical direction at the front, center, and rear is more significant. The roll rate is controlled as well as for the system with active aerodynamic surfaces, and the Pepler index values are considerably lower than either of the other two active systems. According to the Pepler index, the ride quality at the front of the vehicle, despite the high lateral accelerations, is better than average , while at the center of the vehicle it is comfortable. The best ride quality is achieved at the rear of the vehicle.

The air gap variations in both directions are less than those of the passive suspension, while the vertical secondary suspension strokes are higher, but within specifications. The lateral secondary suspension strokes are lower than those of the passive suspension, Since additional resistance to crosswind disturbances can be gained both by making the vehicle's apparent mass larger and effectively making the entire vehicle's yaw and lateral stiffness larger, the secondary suspension stroke variation is reduced.

Note that for the inclusion of guideway disturbances only, all three active control designs resulted in better ride quality at the rear of the vehicle than at the front. This is due to the preview of the rear guideway disturbances from the moment the front bogie experiences them.

Table 5.
Pepler Ride Comfort Index Values
V = 150 m/s (336mph); RMS Wind = 4.8 m/s (10 mph)

	Passive Secondary	Active Hydraulic Secondary	Active Aero-Surfaces	Active Aero & Hydraulic Secondary
Front				
Guideway	3.62	2.05	1.91	1.63
Crosswinds	4.99	3.12	3.23	2.86
Combined	5.97	3.46	3.45	2.96
Center				
Guideway	3.32	1.81	1.60	1.32
Crosswinds	3.61	2.07	1.98	1.88
Combined	4.57	2.38	2.16	1.93
Rear				
Guideway	3.69	1.96	1.70	1.22
Crosswinds	3.52	1.88	1.77	1.48
Combined	4.74	2.33	2.05	1.53

Table 6.
RMS Vehicle Accelerations and Roll Rate
V = 150 m/s (336mph); RMS Wind = 4.8 m/s (10 mph)

	Passive Secondary	Active Hydraulic Secondary	Active Aero-Surfaces	Active Aero & Hydraulic Secondary
Front Y Train Accels				
Guideway	5.32 g/100	4.09 g/100	4.08 g/100	3.23 g/100
Crosswinds	14.26 g/100	11.09 g/100	12.00 g/100	9.81 g/100
Combined	15.22 g/100	11.82 g/100	12.68 g/100	10.33 g/100
Center Y Train Accels				
Guideway	3.89 g/100	2.94 g/100	2.51 g/100	1.42 g/100
Crosswinds	6.19 g/100	4.94 g/100	4.63 g/100	4.05 g/100
Combined	7.31 g/100	5.75 g/100	5.27 g/100	4.29 g/100
Rear Y Train Accels				
Guideway	5.91 g/100	3.65 g/100	2.93 g/100	0.81 g/100
Crosswinds	5.62 g/100	3.84 g/100	3.38 g/100	1.73 g/100
Combined	8.16 g/100	5.29 g/100	4.48 g/100	1.91 g/100
Front Z Train Accels				
Guideway	6.38 g/100	1.76 g/100	1.04 g/100	0.33 g/100
Crosswinds	3.62 g/100	0.71 g/100	0.62 g/100	0.61 g/100
Combined	7.34 g/100	1.90 g/100	1.21 g/100	0.69 g/100
Center Z Train Accels				
Guideway	6.01 g/100	1.50 g/100	0.83 g/100	0.30 g/100
Crosswinds	3.62 g/100	0.71 g/100	0.62 g/100	0.61 g/100
Combined	7.02 g/100	1.66 g/100	1.03 g/100	0.67 g/100
Rear Z Train Accels				
Guideway	6.19 g/100	1.67 g/100	0.99 g/100	0.27 g/100
Crosswinds	3.62 g/100	0.71 g/100	0.62 g/100	0.61 g/100
Combined	7.17 g/100	1.81 g/100	1.17 g/100	0.67 g/100
Roll Rate				
Guideway	1.27 °/s	0.11 °/s	0.07 °/s	0.06 °/s
Crosswinds	1.89 °/s	0.22 °/s	0.17 °/s	0.17 °/s
Combined	2.28 °/s	0.25 °/s	0.19 °/s	0.18 °/s

Table 7.
RMS Air Gap Variations
V = 150 m/s (336mph); RMS Wind = 4.8 m/s (10 mph)

	Passive Secondary	Active Hydraulic Secondary	Active Aero-Surfaces	Active Aero & Hydraulic Secondary
Front Y				
Guideway	0.333 cm	0.424 cm	0.289 cm	0.292 cm
Crosswinds	1.242 cm	1.153 cm	1.254 cm	1.178 cm
Combined	1.286 cm	1.228 cm	1.287 cm	1.214 cm
Rear Y				
Guideway	0.266 cm	0.450 cm	0.269 cm	0.269 cm
Crosswinds	0.355 cm	0.329 cm	0.369 cm	0.307 cm
Combined	0.443 cm	0.557 cm	0.457 cm	0.409 cm
Front Z				
Guideway	0.732 cm	1.346 cm	0.753 cm	0.484 cm
Crosswinds	0.941 cm	0.652 cm	0.714 cm	0.767 cm
Combined	1.192 cm	1.495 cm	1.038 cm	0.907 cm
Rear Z				
Guideway	0.720 cm	1.400 cm	0.756 cm	0.600 cm
Crosswinds	0.094 cm	0.230 cm	0.265 cm	0.216 cm
Combined	0.726 cm	1.419 cm	0.801 cm	0.637 cm

Table 8.
RMS Secondary Suspension Strokes
V = 150 m/s (336mph); RMS Wind = 4.8 m/s (10 mph)

	Passive Secondary	Active Hydraulic Secondary	Active Aero-Surfaces	Active Aero & Hydraulic Secondary
Front Y				
Guideway	0.380 cm	0.642 cm	0.369 cm	0.338 cm
Crosswinds	4.389 cm	5.518 cm	4.473 cm	2.481 cm
Combined	4.406 cm	5.555 cm	4.488 cm	2.504 cm
Rear Y				
Guideway	0.426 cm	1.029 cm	0.414 cm	0.590 cm
Crosswinds	1.132 cm	4.185 cm	1.308 cm	0.133 cm
Combined	1.209 cm	4.310 cm	1.372 cm	0.605 cm
Front Z				
Guideway	1.298 cm	3.362 cm	2.475 cm	2.972 cm
Crosswinds	1.126 cm	1.768 cm	1.321 cm	1.522 cm
Combined	1.718 cm	3.799 cm	2.805 cm	3.339 cm
Rear Z				
Guideway	1.111 cm	3.284 cm	2.427 cm	2.643 cm
Crosswinds	1.598 cm	1.531 cm	0.996 cm	1.088 cm
Combined	1.946 cm	3.623 cm	2.624 cm	2.858 cm

5. CONCLUDING REMARKS

To analyze and quantify the benefits of active control, the authors have developed a five degree-of-freedom lumped parameter modeling capability suitable for a broad class of maglev vehicle and guideway configurations. Perturbation analyses about an operating point defined by train and average cross-wind velocities yield linearized state-space descriptions of the maglev system for multivariable control system analysis and synthesis. Results presented in §4 indicate that the use of active aerodynamic control surfaces, in coordination with the active secondary suspension system, provides significant improvement to the passenger ride quality while ameliorating primary suspension gap requirements. Similar results by the authors ([1], [5], and [6]) for alternative system configurations support this conclusion.

Our analysis and design methodology permits us to alter physical properties, actuation (and potentially, sensing) elements, and disturbance inputs contained within the linear model description. This can be exploited to ascertain optimal system design parameters through parametric trade-off analyses. (We appreciate that specific performance predictions generated by linear analyses should ultimately be verified through high fidelity nonlinear simulation.) A natural extension to our work includes appending additional modeling capabilities, *e.g.*: curved and rolling guideways, vehicle bending modes, actuator and sensor dynamics and noise, and, of course, more sophisticated control techniques.

REFERENCES

[1] *Maglev System Concept Definition*, contract DTFR 53-92-C-00003, prepared by Bechtel/Draper/MIT/Hughes/General Motors for U.S. DOT: FRA.

[2] Wormley, D.N., Young, J.W., "Optimization of Linear Vehicle Suspensions Subjected to Simultaneous Guideway and External Force Disturbances," Journal of Dynamic Systems, Measurement, and Control: Transactions of the ASME, Paper No. 73-Aut-H, March 16,1973.

[3] Guenther, Christian R., Leonides, Cornelius T., "Synthesis of a High-Speed Tracked Vehicle Suspension System - Part I: Problem Statement, Suspension Structure, and Decomposition," IEEE Transactions on Automatic Control, vol. AC-22, No. 2, April 1977.

[4] Gottzein, E.; Lange, B., Ossenberg-Franzes, F., "Control System Concept for a Passenger Carrying Maglev Vehicle," High Speed Ground Transportation Journal, Vol 9, No. 1, 1975, pp 435-447.

[5] Barrows, T., McCallum, D, Mark, S, and Castellino, R. C, *Aerodynamic Forces on Maglev Vehicles,* contract DOT/FRA/NMI-92/21, prepared by C.S. Draper Lab. for U.S Department of Transportation: Federal Railroad Administration.

[6] Mark, Steve, *Modeling and Control of Maglev Vehicles.* Masters Thesis, MIT Department of Mechanical Engineering, 1993.

[7] Thornton, Richard D., "Magnetic Levitation and Propulsion, 1975," IEEE Transactions on Magnetics, Vol. Mag-11, No. 4, July 1975.

[8] Borst. H.V.; Hoerner, S.F., "Fluid-Dynamic Lift," published by Mrs Liselotte Hoerner, Bricktown, NJ, 1975.

[9] Dunlap and Associates, Inc., *Development of Techniques and Data for Evaluating Ride Quality Volume II: Ride Quality Research,* Report No. DOT-TSC-RSPD-77-1, II for U.S. Dept. of Transportation, February, 1978.

[10] Kwakernaak, H., and Sivan, R., *Linear Optimal Control Systems.* New York: Wiley-Interscience, 1972.

[11] Jazwinski, A., *Stochastic Processes and Filtering Theory.* New York: Academic Press, Inc., 1970.